Determination of the interdiffusion coefficient at low temperature in Ni/NiCr nanometer-scale multilayers using X-ray reflectivity

Aurélien Debelle, Anny Michel, Marie Loyer-Prost, Thomas Rieger, Alain Billard, Marylise Nastar

Determination of the interdiffusion coefficient at low temperature in Ni/NiCr nanometer-scale multilayers using X-ray reflectivity

A. Debelle[1,2], A. Michel[3], M. Loyer-Prost[1], T. Rieger[1], A. Billard[4], M. Nastar[1]

1. Université Paris-Saclay, CEA, Service de Recherche de Métallurgie Physique, 91191 Gif-sur-Yvette, France

2. Université Paris–Saclay, CNRS/IN2P3, IJCLab, 91405, Orsay, France

3. Institut PPrime, UPR 3346, Université de Poitiers-CNRS-ENSMA, Chasseneuil-Futuroscope 86960, France

4. FEMTO-ST, UMR 6174 CNRS, MN2S Department, Univ. Bourgogne Franche-Comté, UTBM, Rue Thierry Mieg, 90000, Belfort Cedex, France

Abstract

The interdiffusion coefficient in the Ni/Cr system was determined at low temperature using Ni/$Ni_{0.78}Cr_{0.22}$ nanometer-scale multilayers with periods of 3.65 and 4.50 nm. X-ray reflectivity measurements were carried out to monitor the 1st Bragg peak intensity with annealing time, at both 400 and 450 °C temperatures. The obtained kinetics of the composition modulation decay allowed determining the interdiffusion coefficients of the uniform final solid solution, $Ni_{0.89}Cr_{0.11}$. Values in the order of 10^{-21} to 10^{-20} $cm^2.s^{-1}$ at 400 °C and 450 °C, respectively, were found, in line with extrapolations from data of Cr diffusion obtained at higher temperature.

I. Introduction

Nickel-based superalloys, which exhibit superior mechanical and chemical properties, are broadly used in the aerospace, marine, nuclear reactor, and chemical industries [1, 2]. Among these alloys, Ni-Cr alloys have been extensively explored for their good oxidation resistance (because Cr allows the steel to passivate) and excellent high-temperature strength, which is why they are used in pressurized water nuclear power plants for instance. Under extreme (*i.e.*, mechanical, thermal and irradiation) solicitations encountered in nuclear reactors, chemical potential gradients develop, and atomic interdiffusion takes place. At high temperatures (above 1300 °C), the compound composed of Ni and Cr is a face-centered cubic (fcc) solid solution over a wide range of compositions. However, operating temperatures in the power plants are much lower, and what is more, below those at which thermodynamic and diffusion properties of Ni-Cr alloys have been investigated (because of a small atomic mobility at low temperatures *i.e.*, at a few hundreds of °C). Below 500 °C, the Cr solubility limit and diffusion properties of the Ni-Cr solid solution are hence unknown. Many experimental and theoretical studies have been focused on the atomic short-range order (SRO) in the fcc Ni-Cr solid solutions (see [3] and references therein), and non-trivial variations of the SRO with composition have been highlighted. In particular, there is still no clear relationship between the SRO properties and the first order transition toward a Pt_2Mo-type ordered phase Ni_2Cr [3]. In addition, both density functional theory (DFT) calculations [3] and Calphad energy databases [4] of the Ni-Cr solid solution, show a pronounced local minimum of the enthalpy at a composition around 10 at.% Cr. This enthalpy local minimum could have an impact on the stability of the solid solution and, of greater interest here, on the diffusion driving forces at low temperature. Therefore, determining basic diffusion properties of this particular system (*i.e.*, NiCr alloy with a (final) mean composition around 10 at.% Cr) at temperatures below 500 °C appears to be a crucial issue to tackle.

Diffusion over microns, as that required for conventional techniques, is not possible at low temperatures because it is time prohibitive (reaching full mixing would require months to years of thermal treatment). An original way to circumvent this issue lies in the use of nanoscale multilayers because extremely minute displacements of the diffusing atoms already lead to a significant mixing; this justifies the use of Ni/NiCr nanoscale multilayers here. Then, adapted experimental techniques to detect such extremely short displacements must be implemented, and X-ray reflectivity (XRR), which is highly sensitive to electronic density variation, has shown to be an ideal technique for this purpose. Already in the 1940's, this kind of experiments have been conducted [5]. Since then, several systems have been studied, including Pb/Mg, Au/Ag, Mo/Si, Ti/TiN, Fe/Ni [6-12], and even tailored instrumental set-ups were developed, for instance for *in situ* experiments on a synchrotron beamline [13].

In the presented work, we investigate the Ni and Cr interdiffusion at 400 and 450 °C in the $Ni/Ni_{0.78}Cr_{0.22}$ (initial) system using nanoscale multilayers characterized by XRR measurements and a dedicated analytical model. From the kinetics of the composition modulation decay, we determined

interdiffusion coefficients of the uniform final solid solution, $Ni_{0.89}Cr_{0.11}$. We also compare the obtained values with sets of values that were extrapolated from the high-temperature regime.

II. Experimental details

II.1. Deposition and annealing of the multilayers

The thin films presented in this study were deposited by magnetron sputtering, using the planar deposition technique (i.e. all targets are in the same plane). Two different sets of multilayers were grown, corresponding to different bilayer periods Λ, of nominal values 3.5 nm and 4.5 nm. Hereafter, they will be denominated Λ_L and Λ_S for large and small period, respectively. To prevent any unwanted diffusion at the film/substrate interface during thermal annealing, a diffusion barrier layer was grown on the Si substrate prior to the deposition of the multilayers. For this buffer layer, both SiN_x and SiO_x were used as barriers, and no significant difference in the multilayer growth was found. The total multilayer thickness was chosen to be 1 µm, as the same samples were used for all investigation techniques and in an effort to minimize the influence of the film/substrate interface. Note that the deposition of the samples was done in two steps. First, SiN_x and SiO_x barrier layers (with thickness 150 nm and 300 nm) were deposited onto the Si substrates. Then, substrates coated with a barrier layer were reintroduced in the chamber, and the deposition of multilayers could proceed for both types of barrier-layers concomitantly. A careful cleaning of the surface, as well as a bake-out of the chamber were performed before each multilayer deposition.

The deposition chamber was a stainless-steel cylinder equipped with three circular targets (145 mm in diameter) powered by DC-pulsed (Advanced Energy) generators with a maximum power of 5 kW. The target-to-substrate distance was 7 cm, and the substrates were systematically placed in the sample holder area ensuring a homogeneous thickness, with a lateral variation of less than 5 %. The base pressure of the vacuum chamber reached the value of $6\text{-}7\times10^{-7}$ Pa, which is readily obtained, after a bake-out of the chamber, with the aid of a turbomolecular pump. Such a low base pressure significantly reduces the impurity content of the metallic layers, namely oxygen pollution. During the multilayer growth, the Ar deposition pressure was fixed at a value of 0.2 Pa and the deposition current was fixed at 0.5 A for both Ni and NiCr targets. The planar deposition technique implies that the alternating layers result from the substrate low-speed (1-2 rpm) rotation above the magnetron targets. Thus, a mixing at the layer interfaces can develop due to the widespread angular profile of ejected atoms from the targets; this mixing was minimized by using an aluminum plate in-between the targets, but was eventually observed (see sect. III).

The multilayers were thermally annealed in a tubular furnace under high vacuum (~10^{-4} Pa) at either 400 °C or 450 °C. The temperature was monitored using a type-K thermocouple located in the middle of the heating elements, but not in contact to the sample. Based on tests conducted elsewhere on an equivalent device, the real temperature reached at the sample could be, in this temperature range, around 10 °C lower than the targeted one. In order to limit the time during which the samples would not be at the required

temperature, samples were introduced in the hot zone of the furnace already stabilized at the desired temperature, and they were quickly removed right at the end of the annealing plateau.

II.2. XRD and XRR measurements

The multilayers were characterized using both X-ray diffraction (XRD) and X-ray reflectivity (XRR). For XRD measurements, a D8 Discover Bruker apparatus was used in Bragg-Brentano geometry to record θ-θ scans. The primary optics were composed by a line-focus X-ray tube delivering the two Cu K_α-lines (the K_β radiation was removed using a 3 mm Ni filter) and of 0.4 ° divergence slit, and the secondary optics consisted of a 1D LynxEye detector with a 2.6 ° angular aperture.

For XRR measurements, a 4-circle Seifert XRD3000 diffractometer was used. In this setup, a Cu K_α line-focus X-ray tube, followed by a channel-cut composed of a Ge 220 bi-crystal and a 0.1 mm selection slit, allowed to obtain a parallel monochromatic Cu $K_{\alpha 1}$ beam (λ=0.15406 nm). The detection stage was a 1 mm anti-scattering slit preceding a 0.07 mm detector slit in front of a scintillation detector, yielding an angular resolution of 0.017 °. It is worth mentioning that a knife-edge blade has been used for all measurements; this tool helps to keep the illuminated surface constant when varying the incidence angle, in order to limit artefacts due to surface-related features (e.g. curvature). XRR specular (θ-2θ) scans were recorded using a 0.004 ° step size (in 2θ) and a step time equal to or greater than 10 s.

II.3. TEM and APT analysis

Scanning Transmission Electron Microscopy (STEM) observations and associated Energy Dispersive X-ray spectroscopy (EDX) chemical characterizations were carried out using a FEI Titan3 G^2 80-300 microscope, operated at 300 kV, equipped with a probe corrector and a SuperX Bruker detector. Atom Probe Tomography (APT) analysis was performed using a CAMECA LEAP 4000XHR device at a set point temperature of 50 K in laser pulsing mode at a wavelength of 382 nm, 200 kHz pulse repetition rate. The reconstruction was performed with the commercially available IVAS software. Specimen for both STEM and APT characterizations were prepared using a FIB (Focused Ion Beam) installed on a FEI Helio 650 NanoLab dual-beam scanning electron microscope.

III. Comprehensive description of the multilayer system

First, 150 nm-thick Ni and NiCr monolayers characterized by both XRR and XRD. XRR measurements (not shown here) indicate that the density of both Ni and NiCr is equal to the tabulated bulk density, i.e. 8.9 g.cm^{-3} for the former and 8.5 g.cm^{-3} for the latter with the $Ni_{0.78}Cr_{0.22}$ composition [14]. A significant (topological and/or chemical) roughness was also revealed by these measurements. XRD data are plotted in Fig.1. Although the XRD scans were recorded over a broad 20-90 ° range, only a selected region is presented because the layers exhibit a strong (111) fiber-texture. The corresponding lattice parameter is

found to be equal to the expected one for dense, unstrained material, *i.e.*, 0.3522 nm and 0.3545 nm for Ni and NiCr, respectively [14].

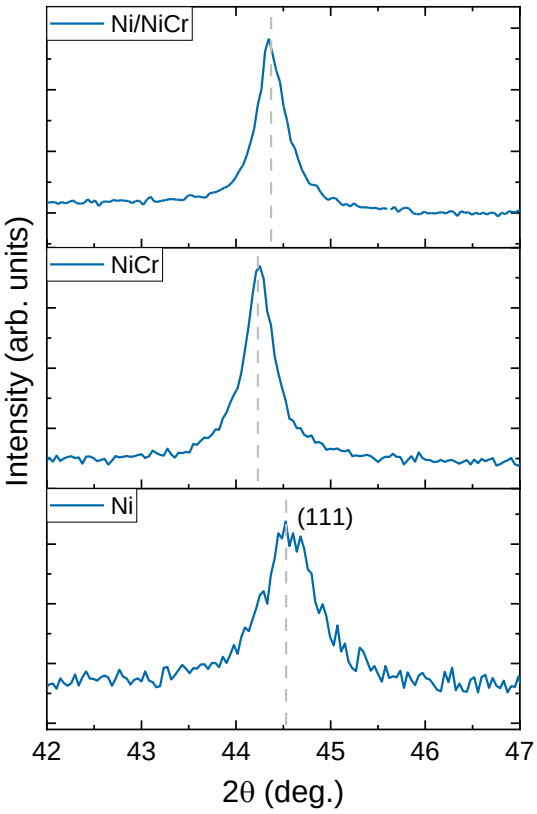

Fig.1: XRD θ-2θ scans recorded on Ni and NiCr reference layers and on a representative Ni/NiCr multilayer. Dashed vertical grey lines indicate the expected (111) peak location for dense, unstrained materials.

Second, both Λ_L and Λ_S multilayers were characterized. The XRD data for the Λ_L multilayer, as representative of both systems, are also displayed in Fig.1. Again, only a narrow region is presented because, as expected from the Ni and NiCr individual layers, the multilayers also exhibit a strong (111) fiber-texture. Furthermore, only the peak corresponding to the average (111) interplanar distance is observed (so-called principal peak [15]), with no (high-angle) superlattice peak. This finding is most likely related to the high roughness of the layers combined with a relatively small period and overlapping diffraction envelops for Ni and NiCr. Nonetheless, the position of the observed XRD peak perfectly corresponds to the weighted average distance of the Ni/NiCr multilayers (thus indicating that the composition is the required one). XRR curves of both Λ_L and Λ_S multilayers are shown in Fig.2. The presence of a 1st Bragg reflection, usually referred to as a (low-angle) superlattice peak, is here observed at 2θ~2.09 ° and 2θ~2.57 ° for the Λ_L and Λ_S multilayers, respectively; it is related to the periodic stacking of the Ni/NiCr bilayers (in other words, the films are definitely multilayers). Taking into account the refraction effect for X-rays at very low incidence angle [16], the period was precisely evaluated from the true 1st Bragg peak position (θ_B) using the following relationship: $\sin^2\theta_B = \sin^2\theta_{exp} - \sin^2\theta_c$, where θ_{exp} is the experimentally determined peak position and θ_c is the critical angle for total reflection. Actual values of 4.50 nm and 3.65 nm were found

for Λ_L and Λ_S, respectively, in good agreement with the nominal values. Note that these values are highly accurate, with a precision better than the angström.

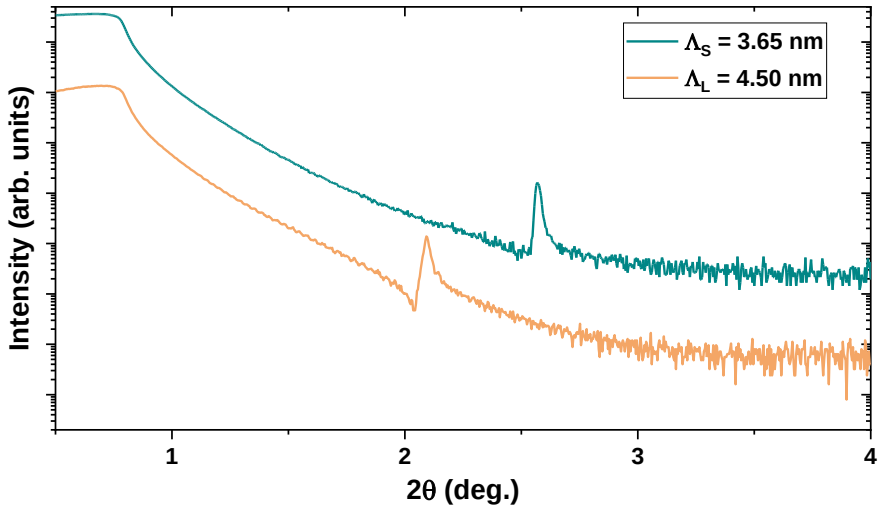

Fig.2: XRR specular θ-2θ scans recorded on as-deposited Ni/NiCr multilayers with both small (Λ_S) *and large* (Λ_L) *periods. Curves are stacked for visualization purposes.*

The absence of higher order reflections can be attributed to several reasons: (i) small multilayer periods (the second-order reflection is expected ~4 ° where the specular intensity is low), (ii) Ni and NiCr layers of equal thickness (which significantly reduces the second-order peak intensity when the number of bilayers is high), (iii) non-abrupt interfaces (which reduces the overall superlattice peak intensity). Note that the latter is an advantage, as a modulation of composition at the interfaces is a crucial condition to apply Fick's law (see sect. IV).

In order to get a better knowledge of our samples, and to provide a direct visualization of the layers, we performed complementary STEM and APT experiments. A STEM image of the as-deposited Λ_L multilayer is presented in Fig.3a, which clearly shows the multilayer stacking but also reveals a columnar structure with elongated grains along the growth direction. The same value of the period as the one obtained from XRR measurements is determined (Λ_L = 4.5 nm). EDX analysis (see Fig.3b) was performed in a region of the sample imaged in Fig.3a: it can be observed that the layers are not perfectly flat and the interfaces not very sharp, which is corroborated by the APT characterization (Fig.3c). The Cr concentration profile, derived from the APT measurements on a sample volume free of 'grain-boundary', is presented in Fig.3d: a sinusoidal-like behavior is observed, with the Cr amplitude ranging from nearly zero in Ni layers to $\simeq$ 22 at.% ($\simeq$ 20 wt.%) in NiCr layers, as expected.

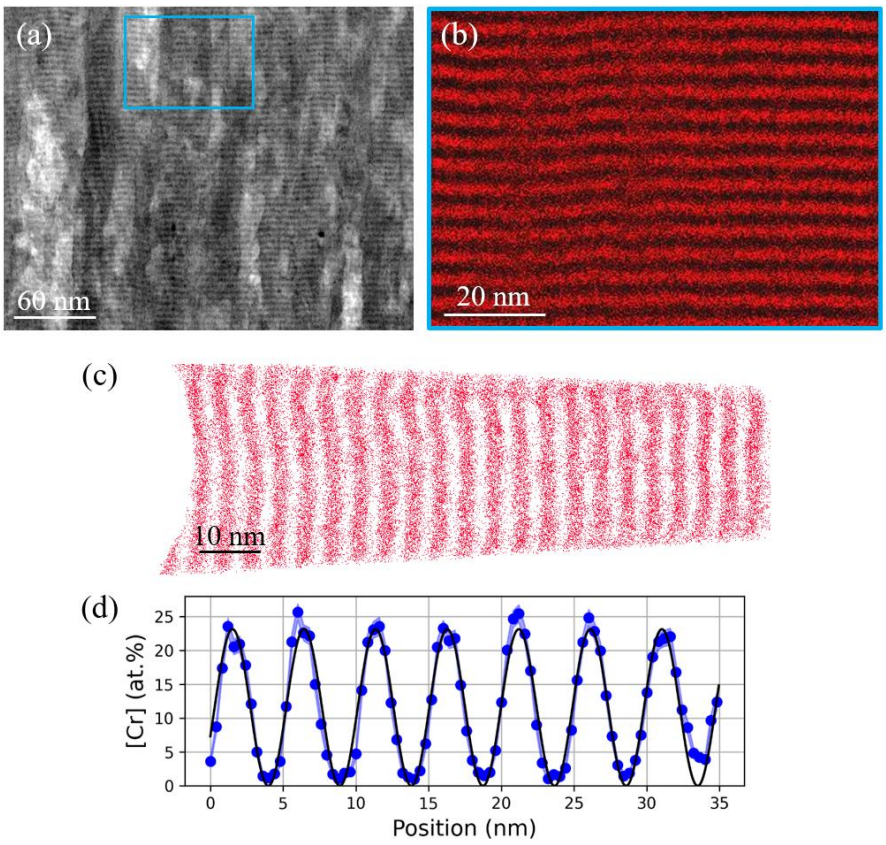

Figure 3: Characterization of the as-deposited Λ_L multilayer. (a) STEM HAADF (High Angle Annular Dark Field) image of the microstructure showing the multilayers and the columnar structure in the growth direction (whose normal is vertical). (b) EDX map showing the Cr distribution (in red) in the multilayers. (c) APT reconstruction of the Λ_L multilayer system showing Cr atoms, (d) corresponding Cr concentration profile (blue points) with the corresponding statistical errors (blue shaded areas) and 'sinusoidal' curve fitting.

IV. Determination of the interdiffusion coefficient

To determine the interdiffusion coefficient, it is not required to fit the XRR curves, as explained hereafter; note that the reliability of those fitted curves is discussed in Appendix A. A simple relationship between the XRR intensity of nanoscale multilayers and the interdiffusion coefficient was already proposed in 1940 by DuMond and Youtz [5], and further commented in details in [12]. They pointed out that a general periodic composition modulation can be described by a Fourier series. The higher harmonics in that series would rapidly decay upon thermal treatment, so that after some interdiffusion the fundamental will be the only significant term. The composition modulation would then become harmonic, and only the first order Bragg reflection would be observed. Hence, assuming that the interdiffusion coefficient, D, is constant, and that the concentration varies with time according to the second Fick's law, the following equation could be used:

$$\mathrm{Ln}\left(I/I_0\right) = -2Dq^2t\,, \qquad (1)$$

In Eq.(1), I_0 and I correspond to the integrated intensity of the 1st Bragg peak before and after annealing, respectively, t is the annealing time, q the scattering vector amplitude ($q=4\pi\sin\theta_B/\lambda$) and D is the interdiffusion coefficient of the final state.

Some limitations and potential artifacts (related to the layer stacking and/or to the studied system and/or to the XRR technique) in the use of Eq.(1) are reviewed in [11]. However, as demonstrated in section III, our multilayers exhibit favorable characteristics that allow to use this relationship, at least to get a relevant order of magnitude of D.

Figure 4 presents the 1st Bragg peak for both Λ_L and Λ_S multilayers and for selected annealing times at 450 °C, obtained after removing the background and normalizing the intensity by the direct-beam intensity. Very slight peak shifts (<0.01 °, i.e. corresponding to maximum two counting steps) are observed but not systematic behavior was detected, so that accuracy of the measurements can most likely account for these shifts. The symmetry of the layered structures and of the diffusion processes requires that the periodicity of the electron density remain unchanged; hence, a constant peak position is here expected. More importantly, it can be readily observed a decrease in the peak integral with increasing time, which is a signature of a chemical composition homogenization.

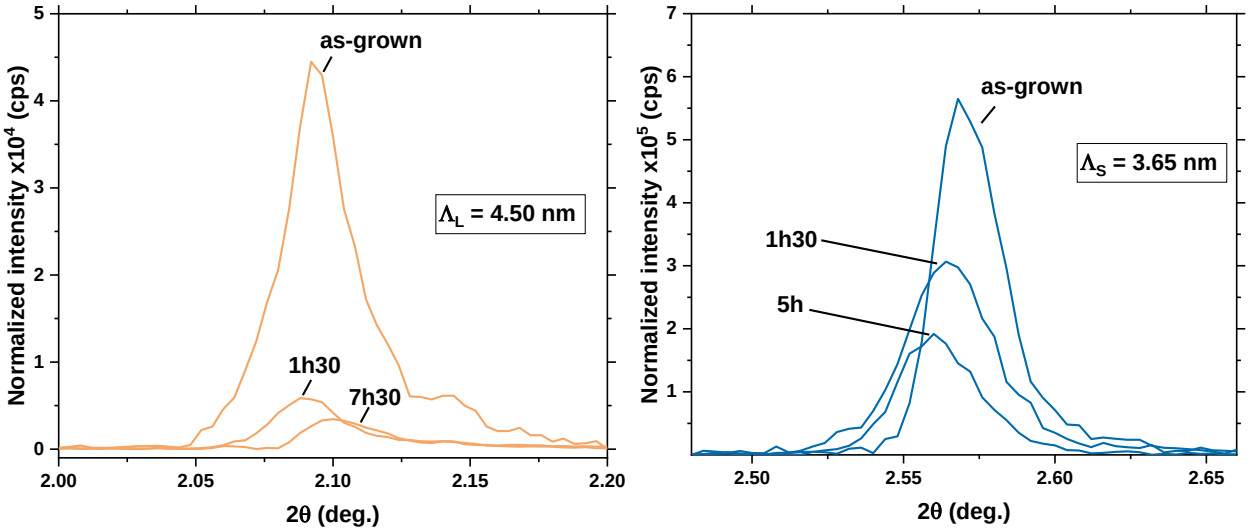

Fig.4: XRR θ-2θ scans, limited to the angular region of the 1st Bragg peak, recorded on pristine and annealed Ni/NiCr multilayers with either small (Λ_S) or large (Λ_L) period. Annealing time is indicated as curve labels.

The variation of the (normalized) peak integrated intensity (in logarithmic scale) as a function of annealing time, for both temperatures, is plotted (symbols) in Fig.5. It is noteworthy that irrespective of the period and of the annealing temperature, there is a significant decrease in intensity after a very short annealing time, i.e. roughly after 1/10th of the time required to reach complete signal disappearance. This first regime in the interdiffusion process is represented by dashed lines in Fig.5. The most probable reason for this extremely rapid intensity drop lies in the presence, in the as-deposited multilayers, of highly-

disturbed regions (identified as grain-boundaries, see Fig.3a) that would act as efficient diffusion pathways. Although only two measurement points are available, we decided to apply Eq.(1) to get a rough estimate of the interdiffusion coefficient in those fast diffusion pathways. Interdiffusion coefficients in the order of 10^{-18} $cm^2.s^{-1}$ at 450 °C and of 10^{-20} $cm^2.s^{-1}$ at 400 °C are obtained (i.e. two orders of magnitude bigger than the values outside these disordered regions, see below). Considering recent results on the diffusion properties at grain boundaries in the NiCr system [17], much larger values could have been expected. In fact, it is most likely that a very short annealing (a few tens of seconds or a few minutes at 450 °C and 400 °C, respectively) would have been sufficient to capture this very fast diffusion process, and hence, would have provided much higher *D* values, but it is unfortunately impossible to carry out such short experiments with a reasonable accuracy on the annealing times.

A second regime, characterized by a much slower intensity decrease, is then observed. It should represent bulk diffusion inside the 'grains'. The solid lines in Fig.5 correspond to linear fitting of the experimental data with Eq.(1). Table I summarizes the corresponding *D* values. The accuracy on these values has been estimated as an overall error that includes, essentially, the calculation of the peak integral, the reproducibility of the experiments (some thermal treatments were repeated twice for this purpose), the slight variation from one sample set to another, and the tiny change in the probed volume between the different samples. The estimated error is about 30 % of the reported values; note that an improved methodology (including the use of thinner, epitaxial layers for instance) is currently being developed to increase this accuracy. Because of kinetic correlation effects and ordering tendency (thermodynamics effects can be neglected due to a high value of the enthalpy second derivative, see section V.), D should increase with Λ [18-19]. However, in this alloy, we anticipate a small, relative increase, in the order of a few percent (as demonstrated in the Appendix B that presents a dedicated mean field calculation). Here, given the precision on the experimental D values, there is no difference between the two multilayer periods. Nonetheless, improving the methodology and considering periods differing by at least a factor 2 could allow accessing the *D* dependence on Λ. Despite the limited accuracy, this work provides the order of magnitude of *D* at low temperature in the $Ni_{0.89}Cr_{0.11}$ system, data that were not available until now: *D* values lie around 10^{-20} $cm^2.s^{-1}$ at 450 °C, and around 10^{-21} $cm^2.s^{-1}$ at 400 °C. Of course, diffusion is significantly slowed down when decreasing the temperature, but the question that arises is how do these values compare with those already available at high temperature? This question is addressed hereafter.

Table I: Interdiffusion coefficients determined from XRR measurements on small and large period multilayers and for two annealing temperatures. Uncertainty on the values was estimated to be 30 %.

	D (450 °C)	**D (400 °C)**
Λ_L (10^{-20} $cm^2.s^{-1}$)	**5.2**	**0.55**

Λ_S (10^{-20} $cm^2.s^{-1}$)	6	0.3

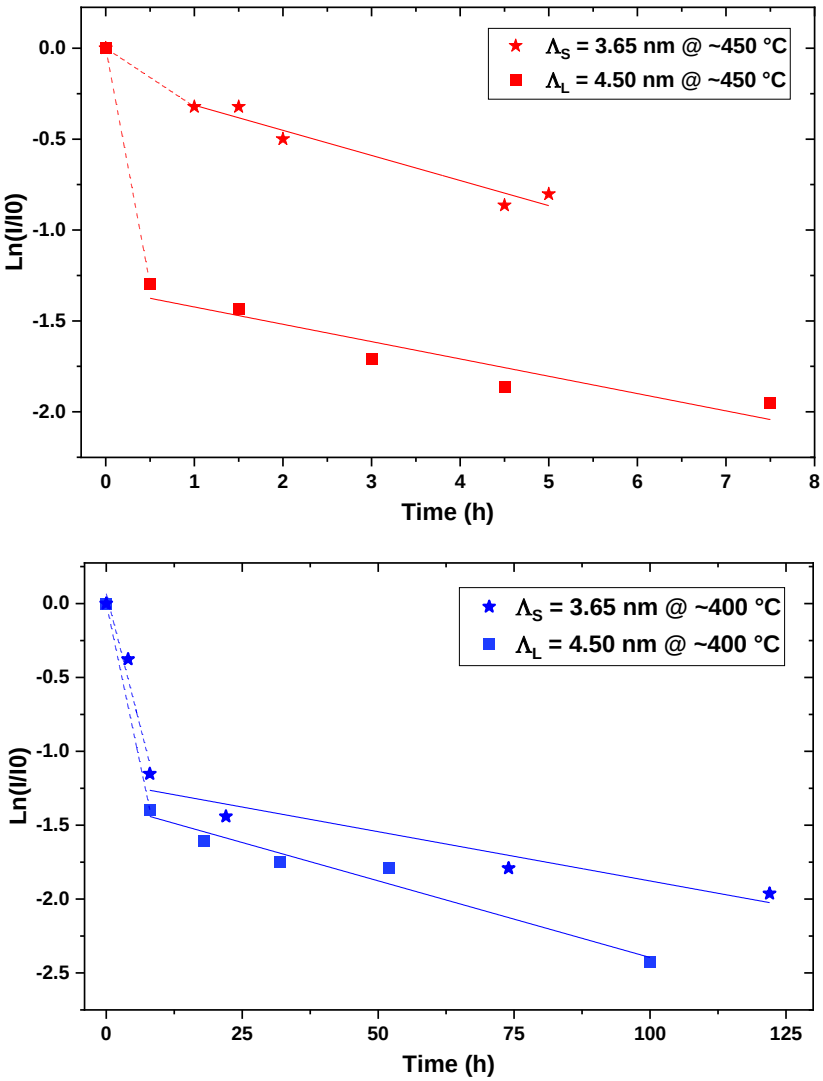

Fig.5: Decay of superlattice 1st Bragg peak intensity as a function of annealing time, for both small and large periods and for 450 °C (a) and 400 °C (b) annealing temperatures.

V. Comparison of the obtained interdiffusion coefficients with extrapolation from high temperature values available in the literature

In the previous section, the decay of the 1st Bragg peak intensity was analyzed until its nearly extinction, which should correspond to a homogenized elemental distribution over the layers: in the case studied here, a composition of 11 at. % Cr will then be reached. Some thermodynamic properties of the NiCr system could have prevented this process, such as the solubility limit or the precipitation of ordered phases. Indeed, a common tangent construction applied to the experimental formation enthalpies of Figure 10 in [3] yields a solubility limit around 10 at. % Cr at 0 K. Furthermore, in Ni-rich metastable solid solutions, the precipitation of Cr-rich random phases may precede the establishment of the Ni2Cr long-range order [20]. Therefore, we might have observed an ordering-decomposition phase transformation: the

extrapolation of the high-temperature phase diagram [14] leads to an expected Cr concentration above 40 at. % in the precipitated ordered phase.

The structural characterization of the as-deposited nanolayers (see section III) points to the stabilization of NiCr solid solutions with a 22 at. % Cr when growth proceeds at room temperature. This stabilization may be linked to the elaboration process, as it is well known that sputter-deposition is a strongly out-of-equilibrium process allowing the stabilization of allotropic phases (see for instance [21] for a review of structural effects during Ta growth). Similarly, the EDX and APT maps on the nano-multilayers presented in Fig. 3 do not reveal any Cr-rich domains. If, however, an ordering-decomposition phase transformation would have occurred during the low-temperature annealing performed in this study, it would have hindered the composition homogenization kinetics, which is in contradiction with the strong logarithmic decrease in the 1st Bragg peak intensity. Consequently, if there were a competition between interdiffusion and ordering kinetics, the present investigation definitely shows that interdiffusion is the dominating process, leading towards a homogenized NiCr solid solution.

Now assuming Cr and Ni diffusion coefficients follow an Arrhenius law with respect to temperature, we can rely on high temperature diffusion data to extrapolate the variation of the bulk interdiffusion coefficient at low temperature. In the binary Ni-Cr alloy, the interdiffusion coefficient is the sum of Ni and Cr intrinsic diffusion coefficients. Since there is no intrinsic diffusion database for this alloy, we introduce the Darken approximation to deduce the interdiffusion coefficient from the Ni and Cr tracer diffusion coefficients, D^*_{Ni} and D^*_{Cr}:

$$D = (C_{Ni}D^*_{Cr} + C_{Cr}D^*_{Ni})\phi \quad (2)$$

with ϕ the thermodynamic factor.

We then write the tracer diffusion coefficients as Arrhenius law:

$$D^*_X = D^0_X exp(-Q_X / RT) \quad (3)$$

where D^0_X is the diffusion pre-factor (including the correlation factor), and Q_X is the activation enthalpy of species X. Note that this simple analytic law ignores the variation of the correlation factor with temperature. We obtain ϕ from the variation of the Gibbs free energy with the alloy composition:

$$\phi = \frac{C_{Ni}C_{Cr}}{k_B T} g'' \quad (4)$$

where g'' is the second derivative of the Gibbs free energy per atom with respect to the alloy composition, i.e. $g'' = \frac{\partial^2 g}{\partial {C_{Ni}}^2}$. Assuming that the configurational entropy of the alloy is the one of a non-interacting ideal solid solution, we derive a direct relationship between ϕ and the second derivative of the enthalpy per atom, h'':

$$\phi = 1 + \frac{C_{Ni}C_{Cr}}{k_B T} h'' \qquad (5)$$

The composition-dependent enthalpy of the Ni-Cr solid solution has been measured at high temperature [4], and also extracted from DFT calculations of random solid solutions [3]. Both approaches highlight the formation of a local minimum of the enthalpy at around 10 at. % of Cr, leading to an unusually high value of the enthalpy second derivative around this composition (which is almost that in our system after chemical homogenization). At $C_{Cr} = 0.11$, h'' is roughly equal to ~ 2.4 eV from experiments, while it is ~ 2 eV when derived from DFT enthalpies (cf. Fig. 10 in [3]). The discrepancy between both values might be due to atomic short-range order effects that are not included in the DFT study, or to the ideal solid solution approximation of the configurational entropy. We chose to keep the experimental value and we neglected its variation with temperature. We then obtained a thermodynamic factor equal to 5.1 and 4.8 at 400 and 450 °C, respectively. Relying on high-temperature tracer diffusion experiments over the full composition range of the Ni-Cr solid solution, Ruzickova and Million [22] have fitted an average composition-dependent Arrhenius law of the Cr and Ni tracer diffusion in binary Ni-Cr alloys. By means of a Calphad method, Jonsson et al. have introduced Cr and Ni mobilities fitted on high-temperature tracer and interdiffusion data of binary and ternary Fe-Ni-Cr solid solutions [23]. More recently, Cr tracer diffusion coefficients down to 542 °C could be measured by Gheno et al. [24]. The reported activation enthalpy of the Cr tracer diffusion coefficient (~270 kJ/mol) is slightly below the average value proposed by Ruzickova and Million (~278 kJ/mol) [22]. Experimental studies systematically report a faster diffusion of Cr than Ni [22]. Thereby, we expect interdiffusion to be controlled by the Cr diffusion, especially at low concentration. Mathematically, we expect the second term in the parenthesis of the RHS of Eq. 2 to be negligible.

As shown in table II, Jonsson's assessment [23] does not reproduce the Cr faster diffusion. Besides, when extrapolated to low temperature, Jonsson's tracer diffusion coefficient of Cr is significantly higher than the experimental reported value [24] and the extrapolation from [22] (see Table II). Therefore, we chose to compare the present results with the low-temperature extrapolations from Ruzickova and Million [22]. We observe that those are below our values. The relative difference is around 20 % at 450°C, and 60 % at 400°C. At 450°C, this relative difference is smaller than the experimental error, which was estimated to be around 30 %. Extrapolations from [22] yield a ratio of interdiffusion coefficients of around 20 between 400 and 450°C, while the present study yields a ratio of ~10, meaning that a better agreement could be obtained if the activation enthalpy of the Cr tracer diffusion coefficient were slightly lower. Nevertheless, in diffusion studies, it is generally considered discrepancies of this order of magnitude to be small. Therefore, the present investigation is a low-temperature validation of the high temperature Cr diffusion Arrhenius law introduced in [22].

Table II: Tracer diffusion coefficients from [22-24] and resulting interdiffusion coefficients deduced from Eqs. (2) and (3). As explained in the main text, the thermodynamic factor, ϕ, is set to 5.1 at 400°C and 4.8 at 450°C. The interdiffusion coefficient resulting from the Cr tracer diffusion coefficient of Gheno et al. [24] does not include the Ni tracer diffusion contribution. The fourth column represents the current experimental results for comparison.

	Ruzickova et al. [22]	Jonsson et al. [23]	Gheno et al. [24]	**This work: Λ_L / Λ_S**
Q_X (kJ/mole)	$Q_{Cr} = 278.4$ $Q_{Ni} = 290$	$Q_{Cr} = 206.6$ $Q_{Ni} = 192.06$	$Q_{Cr} = 270$	/
D_X^0 (cm^2.s^{-1})	$D_{Cr}^0 = 2.26$ $D_{Ni}^0 = 1.71$	$D_{Cr}^0 = 1.49$ $D_{Ni}^0 = 1.90$	$D_{Cr}^0 = 0.4$	/
D_X^* (400 °C) (10^{-20} cm^2.s^{-1})	$D_{Cr}^* = 0.046$ $D_{Ni}^* = 0.004$	$D_{Cr}^* = 1.37$ $D_{Ni}^* = 23.55$	$D_{Cr}^* = 0.044$	/
D_X^* (450 °C) (10^{-20} cm^2.s^{-1})	$D_{Cr}^* = 1.43$ $D_{Ni}^* = 0.16$	$D_{Cr}^* = 14.88$ $D_{Ni}^* = 252.85$	$D_{Cr}^* = 1.25$	/
D (400 °C) (10^{-20} cm^2.s^{-1})	0.21	19	0.23	**0.55 / 0.3**
D (450 °C) (10^{-20} cm^2.s^{-1})	6.1	190	6.0	**5.2 / 6**

Conclusion

In this work, we undertook a study dedicated to determining the interdiffusion coefficient in the Ni/Cr system at low temperature. To this end, we elaborated nanometer-scale multilayers whose initial composition was Ni/$Ni_{0.78}Cr_{0.22}$ and with periods of 3.65 and 4.50 nm. Although it could be expected a precipitation of Cr-rich phases at this Cr concentration, the $Ni_{0.78}Cr_{0.22}$ solid solution was stabilized. We then submitted these samples to thermal treatments at 400 and 450 °C to induce the mixing at the interfaces in the multilayers. No Cr-rich regions were observed after either of these treatments, which indicates that if there were a competition between interdiffusion and ordering kinetics, the former is the dominating process. X-ray reflectivity was employed to monitor the Bragg peak intensity (related to the superlattice) with the annealing in time, which allowed deriving the kinetics of the composition modulation decay. We hence determined the interdiffusion coefficients of the uniform final solid solution, $Ni_{0.89}Cr_{0.11}$. We found values in the order of 10^{-21} to 10^{-20} cm^2.s^{-1} at 400 °C and 450 °C, respectively. No real influence of the period of the multilayers could be detected. These values are in line with extrapolations from data of Cr diffusion obtained at higher temperatures. Finally, it must be mentioned that the proposed methodology can be directly transferred to other systems to quantitatively evaluate such fundamental data.

Acknowledgments

This study has been partially funded by the CNRS-NEEDS program and by the European Commission HORIZON 2020 Framework Program under the grant agreement No. 755269 (GEMMA). Part of the work (FIB and APT experiments) has been carried out in the framework of the French National Research Agency, under the "Investissements d'avenir" program (No ANR-11-EQPX-0020).

Declaration of interest

The authors declare that they have no known competing financial interests or personal relationships that could have appeared to influence the work reported in this paper.

References

[1] R. C. Reed, C. M. F. Rae, Physical Metallurgy (Fifth Edition) 2014, Pages 2215-2290, 22 - Physical Metallurgy of the Nickel-Based Superalloys, Edited by D. E. Laughlin and K. Hono, Elsevier.
[2] L. L. Jun Zhang, C. Ai, Encyclopedia of Materials: Metals and Alloys, Volume 1, 2022, Pages 294-304, Nickel-Based Superalloys, Edited by F. Caballero, Elsevier.
[3] M. Rahaman, B. Johansson, A. V. Ruban, First-principles study of atomic ordering in fcc Ni-Cr alloys, Phys. Rev. B 89, 064103 (2014).
[4] A. Watson and F. H. Hayes, Enthalpies of formation of solid Ni-Cr and Ni-V alloys by direct reaction calorimetry J. Alloy Comp. 220 (1995) 94.
[5] J. Dumond, J. P. Youtz, An X-Ray Method of Determining Rates of Diffusion in the Solid State, J. Appl. Phys. 11 (1940) 357.
[6] J. Dinklage, R. Frerichs, X-Ray Diffraction and Diffusion in Metal Film Layered Structures, J. Appl. Phys. 34 (1963) 2633.
[7] H. E. Cook, J. E. Hilliard, Effect of Gradient Energy on Diffusion in Gold-Silver Alloys, Journal of Applied Physics 40, 2191 (1969).
[8] H. Nakajima, H. Fujimori, M. Koiwa, Interdiffusion and structural relaxation in Mo/Si multilayer films, J. Appl. Phys. 63, 1046 (1988).
[9] S. Chowdhury, R. Gupta, S. Prakash, L. Behera, M. Gupta, Role of interlayer thickness on interdiffusion in Ti/TiN multilayers, Applied Surface Science 564 (2021) 150430.
[10] J. Liu, K. Barmak, Interdiffusion in nanometric Fe/Ni multilayer films, Journal of Vacuum Science & Technology A 33, 021510 (2015).
[11] M. Piecuch, Diffusion in multilayers, Revue Phys. Appl. 23 (1988) 1727.
[12] A. L. Greer, F. Spaepen, Synthetic modulated structures, Eds. I. Chang Leroy and B. C. Giessen (academic press) 1985, p. 419.
[13] J. P. Liu, J. Kirchhoff, L. Zhou, M. Zhao, M. D. Grapes, D. S. Dale, M. D. Tate, H. T. Philipp, S. M. Gruner, T. P. Weihs, T. C. Hufnagel, X-ray reflectivity measurement of interdiffusion in metallic multilayers during rapid heating, J. Synchrotron Rad. (2017). 24, 796–801.
[14] P. Nash, The Cr-Ni system, Bulletin of Alloy Phase Diagrams 7, 466 (1986).
[15] E. E. Fullerton, I K Schuller, H Vanderstraeten, Y Bruynseraede, Structural refinement of superlattices from x-ray diffraction, Phys. Rev. B45 (1992) 9292.
[16] P.F. Miceli, D. A. Neumann, H Zabel, X-ray refractive index: A tool to determine the average composition in multilayer structures, Appl. Phys. Lett. 48 (1986) 24.
[17] T. Gheno, F. Jomard, C. Desgranges, L. Martinelli, Grain boundary diffusion of chromium in polycrystalline nickel studied by SIMS, Materialia 6 (2019) 100283.
[18] J. W. Cahn, Phase Separation by Spinodal Decomposition in Isotropic Systems, J. Chem. Phys. 42 (1965) 93.

[19] M. Nastar, Atomic diffusion theory challenging the Cahn-Hilliard method, Phys. Rev. B 90 (2014) 144101.
[20] L. Karmazin, Lattice parameter studies of structure changes of Ni-Cr alloys in the region of Ni_2Cr, Materials Science and Engineering 54 (1982) 247.
[21] J. Colin, A. Jamnig, C. Furgeaud, A. Michel, N. Pliatsikas, K. Sarakinos, G. Abadias, In Situ and Real-Time Nanoscale Monitoring of Ultra-Thin Metal Film Growth Using Optical and Electrical Diagnostic Tools, Nanomaterials 2020, 10(11), 2225.
[22] J. Ruzickova, B. Million, Self-diffusion of the components in the F.C.C. phase of binary solid solutions of the Fe-Ni-Cr system, Materials Science and Eng. 50 (1981) 59.
[23] B. Jöonsson, Scandinavian Journal of Metallurgy 23, (1994), 201.
[24] T. Gheno, F. Jomard, C. Desgranges, L. Martinelli, Tracer diffusion of Cr in Ni and Ni-22Cr studied by SIMS, Materialia 3 (2018) 145.

Appendix A: Discussion on the fit of the XRR data

In the current work, X-ray reflectivity (XRR) data were not fitted for two reasons.

First, the entire information needed was included in the 1st Bragg peak: its position precisely gives the period, while its integrated intensity is related to the interdiffusion process. In the vast majority of the works where this technique has been used to determine interdiffusion coefficients, the same approach was considered.

Second, the reliability, in the current work, of the fitting results was questionable. Indeed, although it is possible to quite reasonably reproduce the experimental data through a fitting procedure, we established that the accuracy on the obtained (fitting) parameters is not acceptable. To illustrate and support this statement, below are presented a few fitted and simulated curves, taking a multilayer with a 4.50 nm period as an example. XRR calculations have been performed within the Parratt's formalism [1] using the proprietary software called 'Analyze' associated to the Seifert XRR device we used.

In Fig.A1, the results of two reasonably good fitted curves are presented. As one can see, both fitted curves are almost identical, while all major parameters (thickness, roughness and density) more or less differ. The problem obviously lies in the large number of fitting, and usually not independent parameters. In addition to this issue, it can be noticed that for both good fitted curves, a very high roughness is found, similar to the layer thickness. As this parameter includes topological and chemical disorder, it becomes uneasy to use it quantitatively for the purpose of determining the interdiffusion coefficient. In Fig.A2, the period is kept constant while the individual layer thicknesses are reversed: this inversion does not change the computed XRR curve, prohibiting again the use of the obtained values for any quantitative analysis. To finish, it must be pointed out that the XRR data are highly sensitive to the surface oxide layer (see Fig.A3), which inevitably develops during the thermal treatment and hence, hampers a reliable fitting, as more parameters are involved. The lack of accuracy in the fitting parameters lies, in the current work, in the fact that, apart from the 1st Bragg peak (plus the critical angle and the intensity drop), there is no feature to rely on in order to precisely and unambiguously fit the XRR curves. In another, ongoing work, we are currently producing epitaxial (to decrease the initial roughness) and much thinner (to enhance Kiessig fringes) multilayers to improve the reliability of the fitting parameters (thickness, roughness and density) as input for a thermodynamic model of the interdiffusion process.

Table A.1: List of the parameters used or found for the simulation or after the fitting of the XRR curves presented in Figures A1, A2 and A3.

Fit 1					
Layer	**Period**	**Material**	**Density (g.cm^{-3})**	**Thickness (nm)**	**Roughness (nm)**
1		NiO	6.78	1.45	1.25
2	47	NiCr	8.41	2.27	1.73
3	47	Ni	8.90	2.25	1.45
4		NiCr	7.60	∞	2.76
Fit 2					
Layer	**Period**	**Material**	**Density (g.cm^{-3})**	**Thickness (nm)**	**Roughness (nm)**
1		NiO	6.74	1.49	1.25
2	47	NiCr	8.39	2.34	1.61
3	47	Ni	8.90	2.18	1.61
4		NiCr	8.24	∞	2.76
Simulation with a pair of individual layer thicknesses					
Layer	**Period**	**Material**	**Density (g.cm^{-3})**	**Thickness (nm)**	**Roughness (nm)**
1		NiO	6.78	1.45	1.25
2	47	NiCr	8.41	2.52	1.73
3	47	Ni	8.90	2.00	1.45
4		NiCr	7.60	∞	2.76
Simulation with a pair of reversed individual layer thicknesses					
Layer	**Period**	**Material**	**Density (g.cm^{-3})**	**Thickness (nm)**	**Roughness (nm)**
1		NiO	6.78	1.45	1.25
2	47	NiCr	8.41	2.00	1.73
3	47	Ni	8.90	2.52	1.45
4		NiCr	7.60	∞	2.76
Simulation with no surface oxide layer					
Layer	**Period**	**Material**	**Density (g.cm^{-3})**	**Thickness (nm)**	**Roughness (nm)**
1		NiO			
2	47	NiCr	8.41	2.27	1.73
3	47	Ni	8.90	2.25	1.45
4		NiCr	7.60	∞	2.76

References

[1] L.G. Parratt, Surface studies of solids by total reflection of X-rays, Phys. Rev. B 95 (1954) 359.

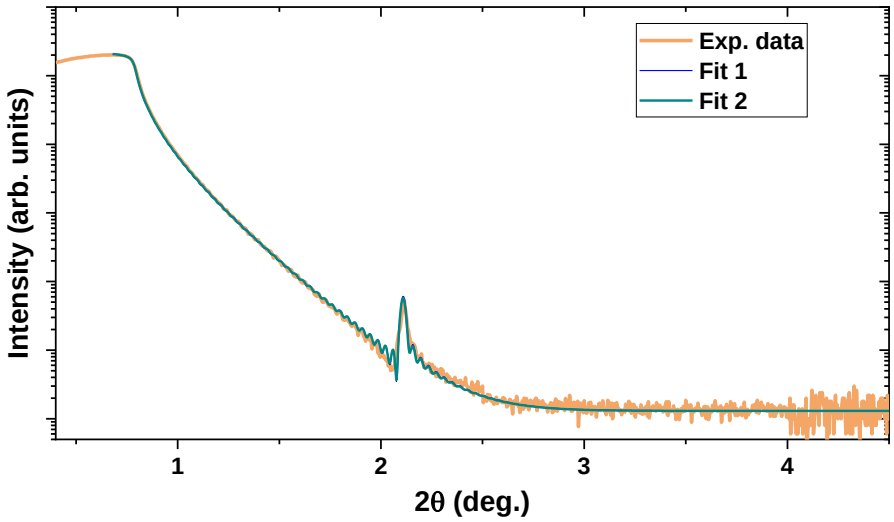

Fig.A1: Experimental XRR curve of an as-deposited Ni/NiCr multilayer of period 4.50 nm, along with two fitted curves providing two different sets of parameters.

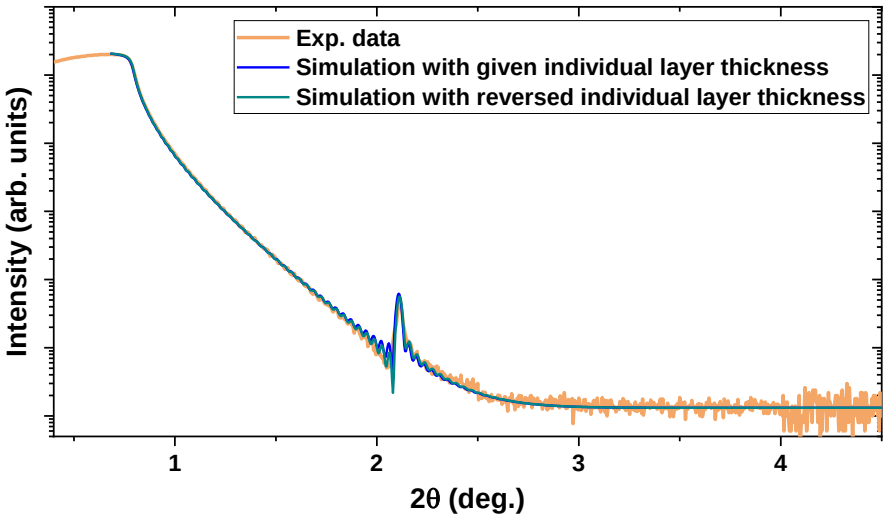

Fig.A2: Experimental XRR curve of an as-deposited Ni/NiCr multilayer of period 4.50 nm, along with two simulated curves obtained by keeping the period constant and reversing the individual layer thicknesses.

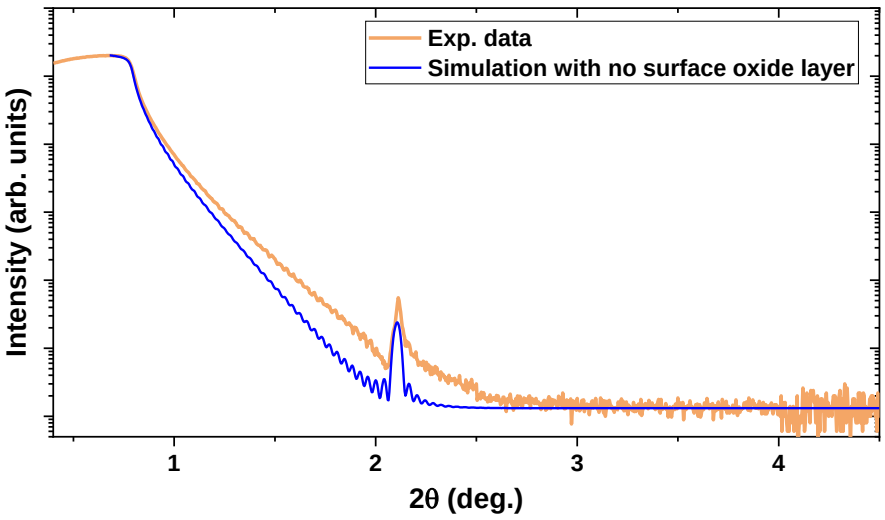

Fig.A3: Experimental XRR curve of an as-deposited Ni/NiCr multilayer of period 4.50 nm, along with a simulated curve where no surface oxide layer.

Appendix B: Modeling of the variation of D with the superlattice periodicity

When the superlattice periodicity is a few lattice parameters in dimension, there is an effect of this periodicity on both the interdiffusion coefficient and the interdiffusion driving force. Phenomenological kinetic models including composition gradient-energy parameters such as the Cahn-Hilliard model predict a linear variation of the effective interdiffusion coefficient with the square of the wavevector [1-2]. Such models are based on a phenomenological expansion of the free energy of the solid solution written as a volume integral of a sum of local bulk and composition gradient energies related to the interface energy. Atomic diffusion mediated by vacancies produces kinetic correlations, which are sensitive to the periodicity of the composition modulation; those correlations reduces the interdiffusion in a non-uniform composition gradient. Yet, we expect a small effect of the kinetic correlations because diffusion coefficients of Cr and Ni are not so different.

Another parameter to consider is the local variation of the concentration gradient that decreases the mixing driving force in alloys with an ordering tendency (as it is the case for the Ni-Cr system). We built-up a mean field method to estimate this thermodynamic contribution to the change in the interdiffusion coefficient with the period. From the reported DFT value of the mixing enthalpy at $C_{Cr} = 0.11$ [3], we may extract a first estimation of the ordering enthalpy. We write the mixing enthalpy as an ordering energy multiplied by the probability of forming attractive Ni-Cr second nearest pairs per lattice site:

$$H = 6C_{Ni}C_{Cr}W$$

with the value '6' being the number of second nearest neighbors in the face-centered cubic structure. At $C_{Cr} = 0.1$, the DFT mixing enthalpy of a random Ni-Cr solid solution is around -0.024 eV [3]. The corresponding ordering energy is then equal to $W = -0.044$ eV. As explained in [5], we may deduce an effective thermodynamic stiffness parameter from the ordering energy, $\kappa = 2W = -0.09$ eV. As expected for a system with an ordering tendency, the thermodynamic stiffness parameter is negative. It yields a relative variation of D equal to:

$$\frac{\Delta D}{D} = \frac{C_{Ni}C_{Cr}}{k_B T}\frac{\kappa}{\phi}$$

with ϕ the thermodynamic factor as defined in Eq. (5). At T=400°C, we obtain $\frac{\Delta D}{D} \approx -0.03$ and at T=450°C, $\frac{\Delta D}{D} \approx -0.04$. Therefore, the resulting relative variation of the interdiffusion coefficient between Λ_L and Λ_S is around one percent. This variation is very small because the thermodynamic factor is abnormally high in this alloy. Consequently, it can be hardly captured in the current experiments.

References

[1] J. W. Cahn, Acta Metallurgica 9 (1961) 795.
[2] J. W. Cahn, J. Chem. Phys. 42 (1965) 93.
[3] M. Rahaman, B. Johansson, A. V. Ruban, Phys. Rev. B 89, 064103 (2014).
[4] M. Nastar, Phys. Rev. B 90 (2014) 144101.